Preprint manuscript submitted to ESSOAr
Pending submission to: *Space Weather Journal* special collection:
"Space Weather Events of 4–10 September 2017"

September 2017's Geoeffective Space Weather and Impacts to Caribbean Radio Communications during Hurricane Response

R. J. Redmon[1], D. B. Seaton[1,2], R. Steenburgh[3], J. He[4], J. V. Rodriguez[1,2]

[1]National Centers for Environmental Information, NOAA, Boulder, CO, USA.

[2]Cooperative Institute for Research in Environmental Sciences, Univ. of CO, Boulder, CO, USA.

[3]Space Weather Prediction Center, NOAA, Boulder, CO, USA.

[4]Massachusetts Institute of Technology and Woods Hole Oceanographic Institute Joint Program in Oceanography and Applied Ocean Science and Engineering, Cambridge, MA, 02139 USA.

Key Points

1. The September 2017 solar events impacted high frequency radio links for ground and aviation communication;
2. Radio communications used in hurricane emergency and disaster relief management were affected, especially in the Caribbean;
3. Active Region AR12673 released 4 X-class flares, 3 coronal mass ejections and a solar energetic particle event with ground level enhancement.

Abstract

Between 4 and 10 September 2017, multiple solar eruptions occurred from active region AR12673. NOAA and NASA's well-instrumented spacecraft observed the evolution of these geoeffective events from their solar origins, through the interplanetary medium, to their geospace impacts. The 6 September X9.3 flare was the largest to date for the nearly concluded solar cycle 24 and, in fact, the brightest recorded since an X17 flare in September 2005, which occurred during the declining phase of solar cycle 23. Rapid ionization of the sunlit upper atmosphere occurred, disrupting high frequency communications in the Caribbean region while emergency managers were scrambling to provide critical recovery services caused by the region's devastating hurricanes. The 10 September west limb eruption resulted in the first solar energetic particle event since 2012 with sufficient flux and energy to yield a ground level enhancement. Spacecraft at L1, including DSCOVR, sampled the associated interplanetary coronal mass ejections minutes before their collision with Earth's magnetosphere. Strong compression and erosion of the dayside magnetosphere occurred, placing geosynchronous satellites in the magnetosheath. Subsequent geomagnetic storms produced magnificent auroral displays and elevated hazards to power systems. Through the lens of NOAA's space weather R-S-G storm scales, this event period increased hazards for systems susceptible to elevated "radio blackout" (R3-strong), "solar radiation storm" (S3-strong), and "geomagnetic storm" (G4-severe) conditions. The purpose of this paper is to provide an overview of the September 2017 space weather event, and a summary of its consequences with forecaster, post event analyst and communication operator perspectives.

1 Introduction

Space weather occasionally occurs in tandem with extreme terrestrial weather. When it does, the struggle to mitigate the impacts to life and property can be dramatically intensified. This one-two punch landed on the socioeconomically and technologically diverse communities of the Caribbean islands during the September 2017 hurricane season. While hurricanes Harvey, Irma, Jose and Maria tore through the Caribbean region, X-class flares, solar energetic particle (SEP) events and Earth-directed coronal mass ejections (CMEs) plowed through the heliosphere. Caribbean emergency communication system operators reported critical impacts to high frequency (HF) radio links used in disaster response and aviation tracking. Unfortunate events such as these provide an opportunity to expand our understanding of critical infrastructure susceptibility to space weather. Such examinations are essential to prepare for and mitigate the impacts of future events. (e.g. Baker et al., 2013; SWAP, 2015). Herein, we explore a diverse suite of research and operational observations and model predictions to provide a comprehensive summary of the evolution of the September 2017 solar eruptive period for the "Space Weather Events of 4–10 September 2017" special collection of the *Space Weather Journal*. The remainder of the manuscript is organized as follows: Section 2 provides an overview, Section 3 describes this space weather period from its solar eruptive origins to the near earth response, Section 4 discusses technological impacts, and Section 5 provides a short summary.

2 September Event Summary

Table 1 captures key space weather, geospace and technological impact details for the ten day period 4–13 September 2017, all originating with solar active region AR12673. The content includes the occurrence of solar flares (≥M5), NOAA Space Weather Prediction Center (SWPC) storm scale alerts for radio blackouts "R", solar energetic particle (SEP) events "S", geomagnetic

storms "G", elevated fluxes of 2 MeV electrons at geosynchronous orbit, coronal mass ejections (CMEs), geostationary magnetopause crossings (GMCs), geomagnetic storm indices, spacecraft hazards, and technological system impacts. Events deemed "strong" are bold (e.g. storm scale level 3) and those deemed "severe" are bold-italic (e.g. storm scale level 4 and infrastructure).

Table 1: Summary of Space Weather 4-13 September 2017 [a]

(1) Date	(2) Flares ≥M5 (begin)	SWPC Storm Scales Alerts				(7) CME Earth-ward	(8) GMC GOES	(9) Geom. Indices (storm time)	(10) Space Haz	(11) System Impacts (Reported, Likely)
		(3) Radio (1–5)	(4) SEP (1–5)	(5) G (1–5)	(6) 2MeV e-					
Sep-4	M5.5 (20:28)	R2			**Yes**	Ejected (CME0)			IC	
Sep-5			S2	G1	**Yes**				IC	
Sep-6	**X2.2 (08:57)** **X9.3 (11:53)**	**R3**	S2		**Yes**	Arrived (CME0) Ejected (CME1)			IC	***HF Ground (reported)*** ***HF Aviation (reported)***
Sep-7	M7.3 (10:11) **X1.3 (14:20)**	**R3**	S2	G3	**Yes**	Arrived (CME1)	**Yes**	Sep-8: Kp_{max} 8.3 Dst_{min} -142 nT (quick-look) -234 nT (predicted)	IC	
Sep-8	M8.1 (07:40)	R2	S2	***G4***	**Yes**				IC	**WAAS and EGNOS LPV** (likely)
Sep-9					**Yes**				IC	
Sep-10	**X8.2 (15:35)**	**R3**	**S3, Yes GLE72**		**Yes**	Ejected (CME2)			IC SEE	***HF Ground*** (reported)
Sep-11					**Yes**				IC SEE	
Sep-12			S2	G1	**Yes**	Arrived			IC	

Sep-13			S1	G1		(CME2)				

[a] The 11 columns are laid out thus: (1) date, (2) flares (≥M5), (3) radio storm scale "R", (4) solar radiation storm scale "S" and >100 MeV protons exceedance of 1 pfu (Yes or blank), (5) geomagnetic storm scale "G", (6) 2 MeV electron alert, (7) CMEs, (8) GMC, (9) storm-time extrema in Kp and Dst, (10) space asset hazards, (11) system impacts. The Dst_{min} "quick-look" is from the Kyoto World Data Center (WDC), and "predicted" is from LASP (Temerin and Li [2002, 2006]).For the three SWPC storm scales in columns 3–5, only the greatest space weather scale value is listed in cases where multiple same-category alerts were issued for a given day. Entries deemed "strong" are **bold** and those deemed "severe" are ***bold-italic***.

Through its eruptive evolution, AR12673 produced four X-class flares (column 2), with the most significant being an X9.3 on 6 September and an X8.2 on 10 September. In response, SWPC forecasters issued alerts for R3 "strong" radio blackouts (column 3). Reports of high frequency (HF) radio impacts were received from emergency communication providers such as the Hurricane Watch Net (HWN) and aviation interests such as the French Civil Aviation Authority (DGAC). The 10 September eruption resulted in the first SEP event with a ground level enhancement (GLE) near sea level since 2012 (Mishev et al., 2017), now known as GLE 72 (column 4). Several significant CMEs with at least partial earthward trajectories were emitted. Since this text is focused on the 6 and 10 September eruptions, we have named the CMEs as CME0 (4 September), CME1 (6 September) and CME2 (10 September) (column 7). The arrival of CME1 on 7-8 September heralded a very significant compression/erosion to the dayside magnetosphere, enough so to place geosynchronous spacecraft into the magnetosheath (column 8). CME1 prompted a G4 "severe" SWPC alert (column 5) with a moderate overall geomagnetic storm (Kp_{max} 8.3; Dst_{min} -142 nT (quick-look), -234 nT (predicted)) (column 9). With respect to 2 MeV electrons (column 6), known to be important for spacecraft internal charging considerations (column 10), this period extends a fairly long run of elevated 2 MeV electrons, with the alert threshold exceeded semi-continuously as far back as mid July.

For this paper we used data derived from National Oceanic Atmospheric Administration (NOAA) SWPC and the National Centers for Environmental Information (NCEI), and National Aeronautics and Space Administration (NASA) archives. All of these data are publicly available (see Table 2). The knowledge accumulated in Table 1 is afforded through collaboration and leveraging of several key communities. Space weather practitioners must integrate disparate data into a synthesis describing the current and future state of the space environment, distilling the results with an eye towards the technological and societal impacts. They do this continuously during their shift, across spatial and temporal scales spanning several orders of magnitude. (Figure 1). Forecasters issue an *Alert* to "indicate that the observed conditions, highlighted by the warnings, have crossed a preset threshold or that a space weather event has already started", a *Watch* "when the risk of a potentially hazardous space weather event has increased significantly, but its occurrence or timing is still uncertain.", and a *Warning* "when a significant space weather event is occurring, imminent or likely. A Warning is a short-term, high confidence prediction of imminent activity." (SWPC, 2018). In summary, Table 1 is made possible by the real-time SWPC forecaster synthesis of observations (Figure 1) from NOAA and NASA spacecraft (Figure 2) and ground platforms (e.g. magnetometers) into space weather alerts, watches and warnings; the awareness of technology operators to report issues broadly for awareness and additional perspective; and long term space environment scientific stewardship.

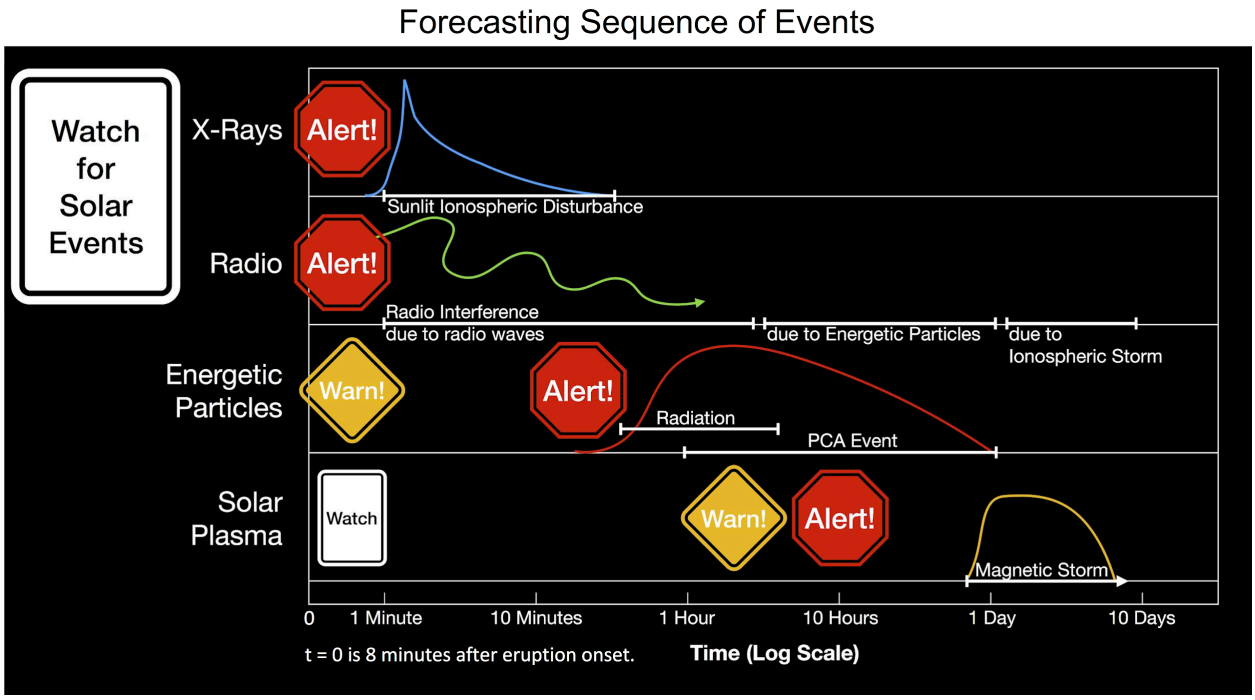

Figure 1: A forecaster's timeline. SWPC and other forecasters are always watching for solar events as potential predictors of near-term technological impacts. This diagram provides a rough phenomenological timeline from X-ray and radio noise producing flares (top) to energetic particles (i.e., SEPs of both eruptive and CME origin) and the arrival of CME solar plasma. *Watches*, *Warnings* and *Alerts* are invaluable tools for forecasters to dissemination critical space weather information. Adapted from SWPC's "Time Scale for Solar Effects".

3 Sun to Earth: Solar origins to Geospace response

In this section, we present a Sun to Earth perspective, using data from several satellites (Figure 2). From our sunward observation location, the Lagrange point L1, we have solar imagery of the corona provided by NASA's Solar and Heliospheric Observatory (SOHO) satellite; and in situ measurements of passing solar wind from the NOAA Deep Space Climate Observatory (DSCOVR) and the NASA Advanced Composition Explorer (ACE), SOHO, and Wind satellites. In geosynchronous orbit, NASA's inclined (28.5°) Solar Dynamics Observatory (SDO) provides solar imagery of the disk, while NOAA's Geostationary Operational Environmental Satellites (GOES) provide solar imagery and in situ measurements of the penetrating and trapped particle

130 and magnetic field environment.

131

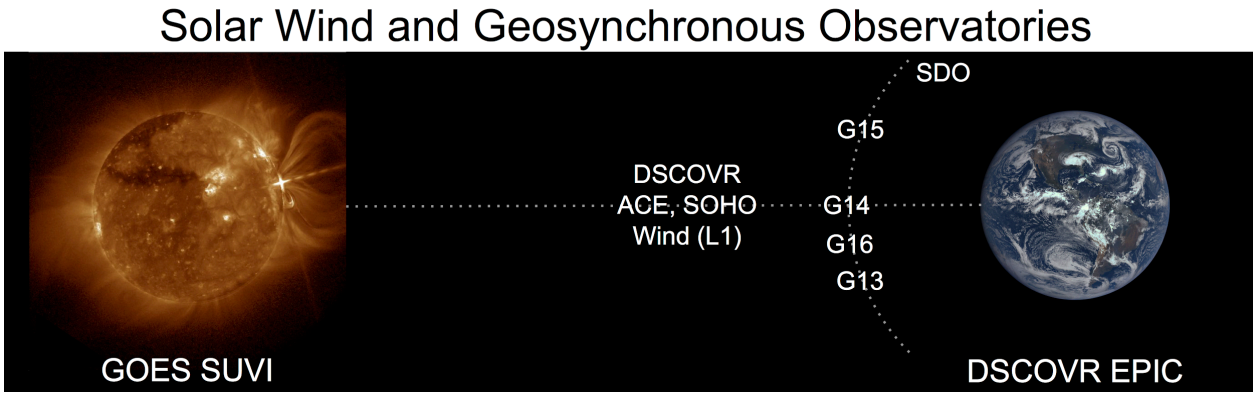

132
133 Figure 2: Solar wind and geosynchronous observatories used in the present study. The nine
134 DSCOVR, ACE, SOHO, Wind, SDO, and GOES (G13–G16) satellite notional locations are
135 shown from the perspective of an observer looking down on the Sun-Earth ecliptic plane. At the
136 time of the September events studied here, the GOES spacecraft were located at these
137 approximate west geographic longitudes: 75 (G13), 90 (G16), 105 (G14), 135 (G15). The G16
138 SUVI image (left) captures the 10 September solar eruption (15:58 UT), while the DSCOVR
139 EPIC image (right) captures the Americas on 11 September 2017. (Image is not to scale.)
140

141 The early life of solar active region AR12673 was not initially suggestive of its rapid and
142 explosive evolution as it rotated across the solar disk. Figure 3 reveals the time history of
143 AR12673 and its eruptive events on 6 and 10 September. The top row provides the eight day
144 time evolution covering 3–10 September from the SDO Atmospheric Imaging Assembly (AIA)
145 instrument, with AR12673 circled in the 3 September image. From 2 to 3 September, AR12673
146 expanded dramatically in both size — by roughly a factor of ten — and magnetic complexity.
147 Between 4 and 10 September, it fired off four X-class (X2.2, X9.3, X1.3, X8.2 in chronological
148 order) and numerous ≥M5 class flares (see Table 1). The two pairs of images in the middle row
149 show the solar disk at a wavelength of 195 Å from the new GOES-16 Solar Ultraviolet Imager
150 (SUVI) aboard GOES-16 and coronagraphic images of ejecta from the SOHO Large Angle and
151 Spectrometric COronagraph (LASCO) (C2) for the 6 and 10 September events, respectively.
152 GOES-16 is the first in the NOAA GOES-R series of four spacecraft and was located at roughly

153 90° west geographic longitude for these events and most of 2017. The LASCO images reveal the
154 massive ejecta emitted on these days, with the 6 September eruption's CME resulting in intense
155 magnetospheric compression and a G4 "severe" alert (Figure 5 and Table 1). The bottom row
156 shows the matching X-ray light curves observed by the GOES-15 X-ray Sensor (XRS)
157 instrument's "long" band (1 to 8 Å). SWPC uses XRS measurements to determine the radio
158 blackout scale (R) and these events resulted in R3 "strong" alerts (Table 1). The SUVI images
159 are taken at the time nearest to the X-ray peaks for the given event. Collectively, this active
160 region's explosive events on 6 and 10 September are the most energetic of solar cycle 24 (Seaton
161 and Darnel, 2018).
162

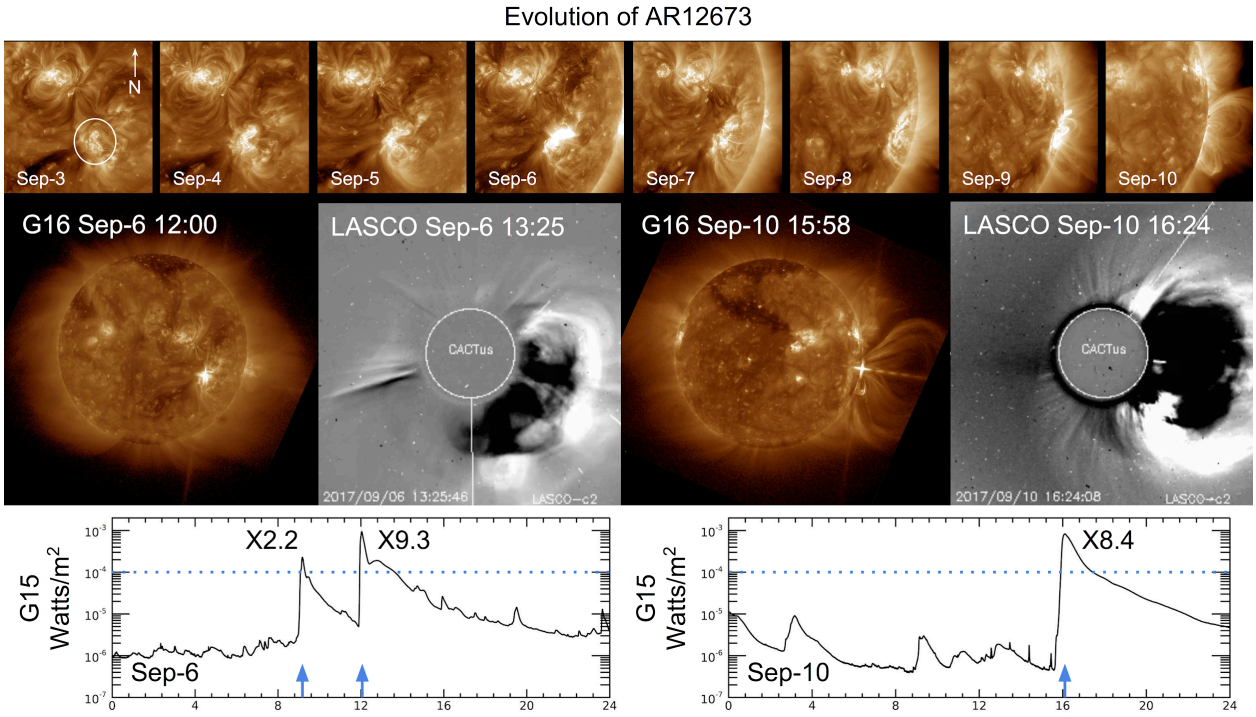

163
164 Figure 3: The evolution and eruptions of Active Region AR12673. The top row shows the time
165 evolution of AR12673 covering 3 September (circled) through 10 September by SDO AIA's 193
166 Å telescope. The middle row shows the 6 and 10 September eruptive events as recorded by
167 GOES-16 SUVI (195 Å) and SOHO LASCO (C2). SUVI images are after Seaton and Darnel
168 (2018). The LASCO images were created using the Computer Aided CME Tracking CACTus
169 package (Robbrecht and Berghmans, 2004). The bottom row reveals the X-ray light curves
170 captured by GOES-15 XRS (0.1-0.8 nm "long") covering 6 and 10 September and blue arrows

mark the times of peak irradiance for the 3 X-class flares shown here. Brief outages of GOES-15 XRS near 9UT due to eclipse have been filled using GOES-13. The X1.3 flare on 7 September is not shown here.

Active region AR12673 erupted several times between 4 and 10 September, producing enhancements in the SEP population originating from the solar eruption site as well as energization by subsequent propagating CMEs, resulting in several SWPC solar radiation storm scale "S" alerts ranging from moderate (S2) to strong (S3) (Table 1). Figure 4 shows GOES-13 measurements of the SEP protons penetrating through the geomagnetic field (top left) and trapped electrons (bottom left); and an evaluation of the GLE 72 event onset as observed by multiple GOES spacecraft and ground based neutron monitors (NMs) (right column). The top left plot shows proton fluxes in the energy range of >5 MeV to >100 MeV observed by the GOES-13 Electron, Proton, Alpha Detector (EPEAD). The measurements from the westward-viewing telescopes for EPEAD are shown here because they observe larger solar proton fluxes than the eastward view due to the former seeing particles whose gyro centers lie outside geosynchronous orbit and are hence less filtered by the geomagnetic field (e.g., Rodriguez et al., 2010). Several SEP enhancements are annotated by their cause, solar eruption (September 4, 6 and 10) or CME1 or CME2 energized (September 7 and 8, and 12), in agreement with the findings of Schwadron et al. (2018) through their analysis of the Cosmic Ray Telescope for the Effects of Radiation (CRaTER) detector. The period September 5–15 elevated the risks of astronaut radiation, space hardware Single Event Upsets (SEUs) and high latitude trans-ionospheric radio absorption.

The eruption on 10 September propelled relativistic ions and electrons outward from AR12673 resulting in the first solar energetic particle (SEP) event with sufficient energy to yield a ground

196 level enhancement (GLE) in the count rates of secondary neutrons observed near sea level since
197 2012. This SEP event is now known as GLE 72 (https://gle.oulu.fi/#/). According to Schwadron
198 et al. (2018), GLE 72 "had an unusually hard spectrum, with large fluxes above 400 MeV, and
199 large dose rates in the most shielded CRaTER detector." The CRaTER instrument is on the
200 Lunar Reconnaissance Orbiter (LRO) in orbit about Earth's moon, and observes SEP events
201 essentially unfiltered by a planetary magnetosphere (Huang et al., 2009), unlike GOES.
202 Schwadron et al. provide concrete evidence that the multiple eruptions of AR12673 prior to 10
203 September created an interplanetary SEP seed population that was further energized by the 10
204 September eruption, in concurrence with past multi-CME studies (e.g. Li et al., 2012; Lugaz et
205 al., 2017). Evaluation of GLE 72's event onset detectability at Earth by GOES-13,14,15 and six
206 NM ground stations is presented in the right column. The technique used here for GLE 72 is the
207 same as that of He and Rodriguez (2018), who studied 17 GLEs, GLE 55 (November 6, 1997)
208 through GLE 71 (May 17, 2012) using an adaptation of the running-average detection method of
209 Kuwabara et al. (2006) designed to detect event onsets in noisy 1-min-cadence time series data,
210 and comprehensively concluded that neutron monitor and GOES observations detected similar
211 onset times; the 25th, 50th and 75th percentile differences being -1.5, 0, and +2.5 min when
212 GOES and NMs were compared using the same alert protocol. In the current study, we find that,
213 among the ensemble of measurements shown in Figure 4, GLE 72 was detected first by the
214 GOES-13 HEPAD P10 channel at 1618 UT, followed closely by the Fort Smith NM at 1619, the
215 GOES-14 HEPAD P9 and GOES-15 HEPAD P10 channels at 1620, and the EPEAD P7
216 channels on all three satellites at 1622. Interestingly, the next two NM detections were at 1648
217 and 1652, by the Oulu and Terre Adélie NMs respectively, followed by South Pole Bare at 1657,
218 and Mawson at 17:02. These delays with respect to the Fort Smith detection indicate a

pronounced anisotropy in the SEP event fluxes at onset.

Radiation belt electrons (Figure 4 bottom left) were elevated for much of the 2017 summer, with the SWPC alert threshold exceeded (>2MeV, >1000 pfus) semi-continuously as far back as mid-July. The population was increased considerably (red trace enhancement on 8 September) by the moderate geomagnetic storm on 7–8 September (Kp_{max} = 8.3; Dst_{min} = -142 nT (quick-look), -234 nT (predicted)) (Table 1). Typical spacecraft shielding can be penetrated by MeV electrons and thus spacecraft immersed in such environments for long periods risk degradation and permanent damage through long term dose and internal electrostatic discharge (Bodeau, 2010; Wrenn and Smith, 1996). It is worth pointing out that the solar proton population on 10–12 September strongly contaminated the EPEAD electron >4 MeV channel measurements (Figure 4, bottom left, green trace) and the >2 MeV channel less obviously but still substantially. The contamination in these channels was smaller though not negligible on 6–8 September. In contrast, the >0.8 MeV channel was negligibly contaminated by these SEP events and therefore can be used to monitor unambiguously the evolution of the outer radiation belt at geostationary orbit throughout this period. The arrivals of ICME0, ICME1, ICME2 and SIR1 on 6, 7,13, and 14 September, respectively, caused dropouts in the electron fluxes as expected (e.g., Onsager et al., 2007). Although the increase following the storm on 7–8 September triggered by the first two ICMEs was substantial, as noted above, the electron fluxes at all three energies (>0.8, >2 and >4 MeV) increased to greater than pre-event (4 September) levels following the arrival of SIR1. The dynamics of the magnetosphere and the radiation belts in response to the arrival of these three ICMEs and one SIR is a rich case deserving of in-depth study.

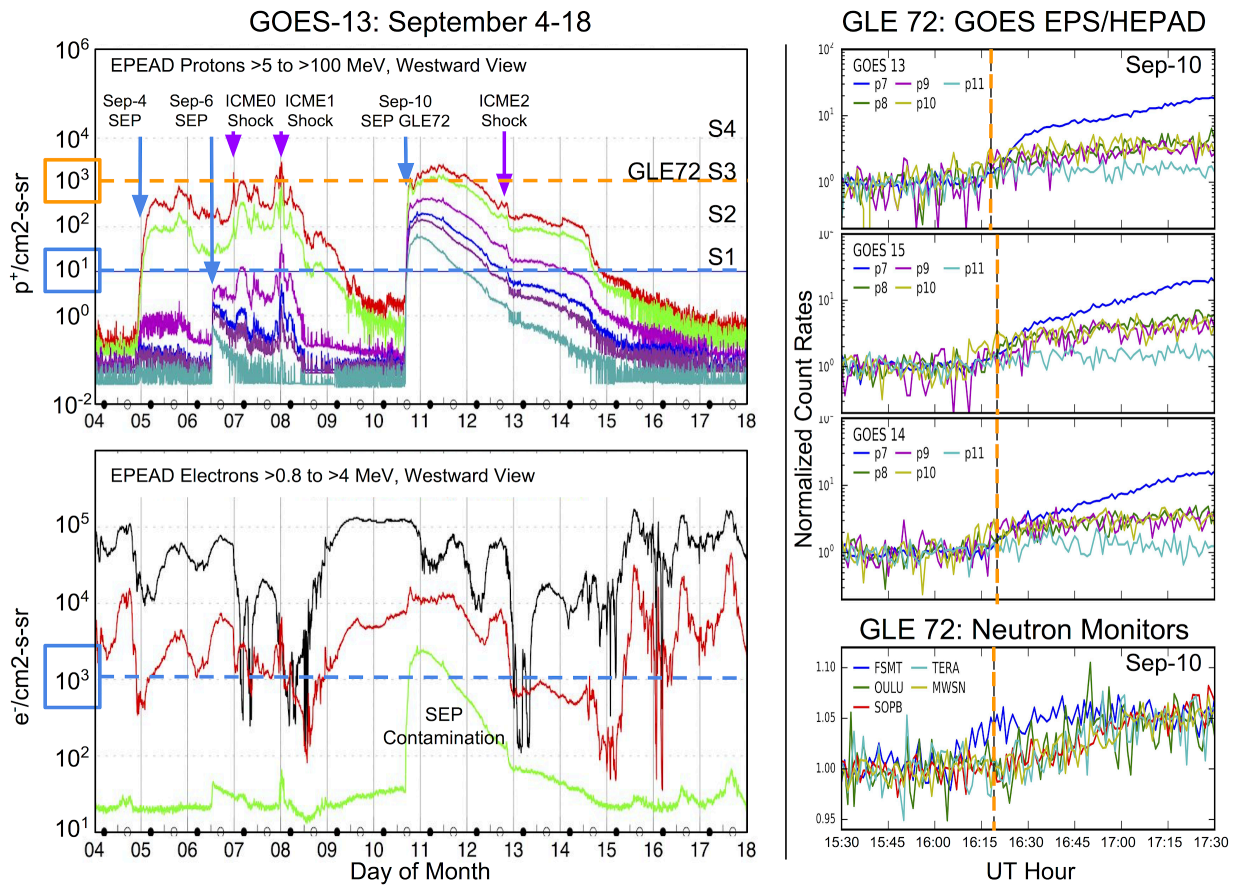

Figure 4: Solar energetic particles, GLE 72, and trapped electrons. The left column shows proton (top) and electron (bottom) fluxes for September 4–18 from the GOES-13 EPEAD westward directed telescope. The top figure shows protons for the 6 integral MeV energy ranges: >5 (*red*), >10 (*green*), >30 (*magenta*), >50 (*blue*), >60 (*purple*), and >100 (*cyan*). The 3 SEP event onsets from solar eruptions on 4, 6, and 10 September are indicated by vertical arrows, with the >10 MeV channel (green) exceeding the SWPC S-scale S1 alert threshold for several days between 5–15 September (inclusive) (blue dashed). The bottom figure shows electrons for the 3 integral MeV ranges: >0.8 (*black*), >2 (*red*), >4 (*green, SEP* contaminated). The dashed blue line here is the SWPC alert threshold for >2 MeV electrons (*red* curve). The right column depicts the September 10th, GLE-72 SEP event onset (*orange*) observed by GOES-13,14,15 and six NM ground stations from 15:30–17:30 UTC. The five GOES-13–15 channels shown here are from the EPS (P7, aka dome 5) and HEPAD (P8–P11, zenith directed telescope) instruments, collectively representing the nominal energy range >110 to >700 MeV. The five NMs are Fort Smith (FSMT), Oulu (OULU), South Pole Bare (SOPB), Terre Adélie (TERA), and Mawson (MWSN).

As summarized in Table 1, active region AR12673 ejected three CMEs during the period of 4–10 September. Their propagation through the interplanetary medium resulted in additional SEP enhancements (Figure 4) and their impingement on geospace resulted in compression and

erosion of the magnetopause inward of geostationary orbit, a "severe" SWPC geomagnetic alert (G4) and a moderate geomagnetic storm (Kp_{max} 8.3; Dst_{min} -142 nT (quick-look), -234 nT (predicted)). Observations of key solar wind bulk plasma parameters propagated to the bowshock nose, the geomagnetic condition and the dayside magnetosphere response to ICME1 (arriving on 7 September) and ICME2 (arriving on 12 September) are captured in Figure 5. The top four plots are the bowshock plasma parameters: IMF Bz, flow speed, density, and the estimated bowshock nose distance. The next two plots are the Kp and Dst indices. The vertical, dashed, blue lines signal the arrive of ICMEs and SIRs at the bowshock nose. The 9 September bowshock data gap is currently under investigation. As proxy for the solar wind condition during this outage, the geomagnetic storm which peaked on 8 September, is well into recovery phase by the 9 September start of the outage. Finally, the lower quad of four plots shows the GOES-13 and GOES-15 magnetic field in a dipole aligned frame.

The arrival of ICME1 (7 September, second dashed line) resulted in compression and erosion of the dayside magnetosphere, with the bowshock nose estimated to be ~ 7.5 Re (geocentric) (fourth plot from top) (Farris, M.H. and C.T. Russell, 1994) and GMCs observed episodically by GOES. These GMCs were observed for about 2.5 hours on the dusk flank (lower left plot, orange interval) at the 7 and 8 September boundary by GOES-15 (lower left plot, orange interval), and for about 1.8 hours later on 8 September by GOES-13 (left, second from bottom) via the GOES magnetometer criteria ($B_h < 0$ nT). The arrival of ICME2 (12 September, third blue dashed line) resulted in much less predicted compression and erosion, and in concurrence, GOES-13 and GOES-15 which were also on the dayside at the time of arrival did not observe entry into the magnetosheath by the same magnetometer criterion. The IMF Bz was much more southward and

the flow speed much stronger for the arrival of ICME1 (7 September) than for ICME2 (12 September) (topmost two plots). Looking forward to future capability, GOES-16's new Magnetospheric Particle Sensor-Low (MPS-LO) (Dichter et al., 2015) will provide electron and ion density and temperature moments to improve the detection of GMCs beyond the traditional criteria used here (i.e., Suvorova et al., 2005). The new moments and magnetopause location products will be transitioned from NCEI and used operationally by SWPC (i.e., Petrinec et al., 2017).

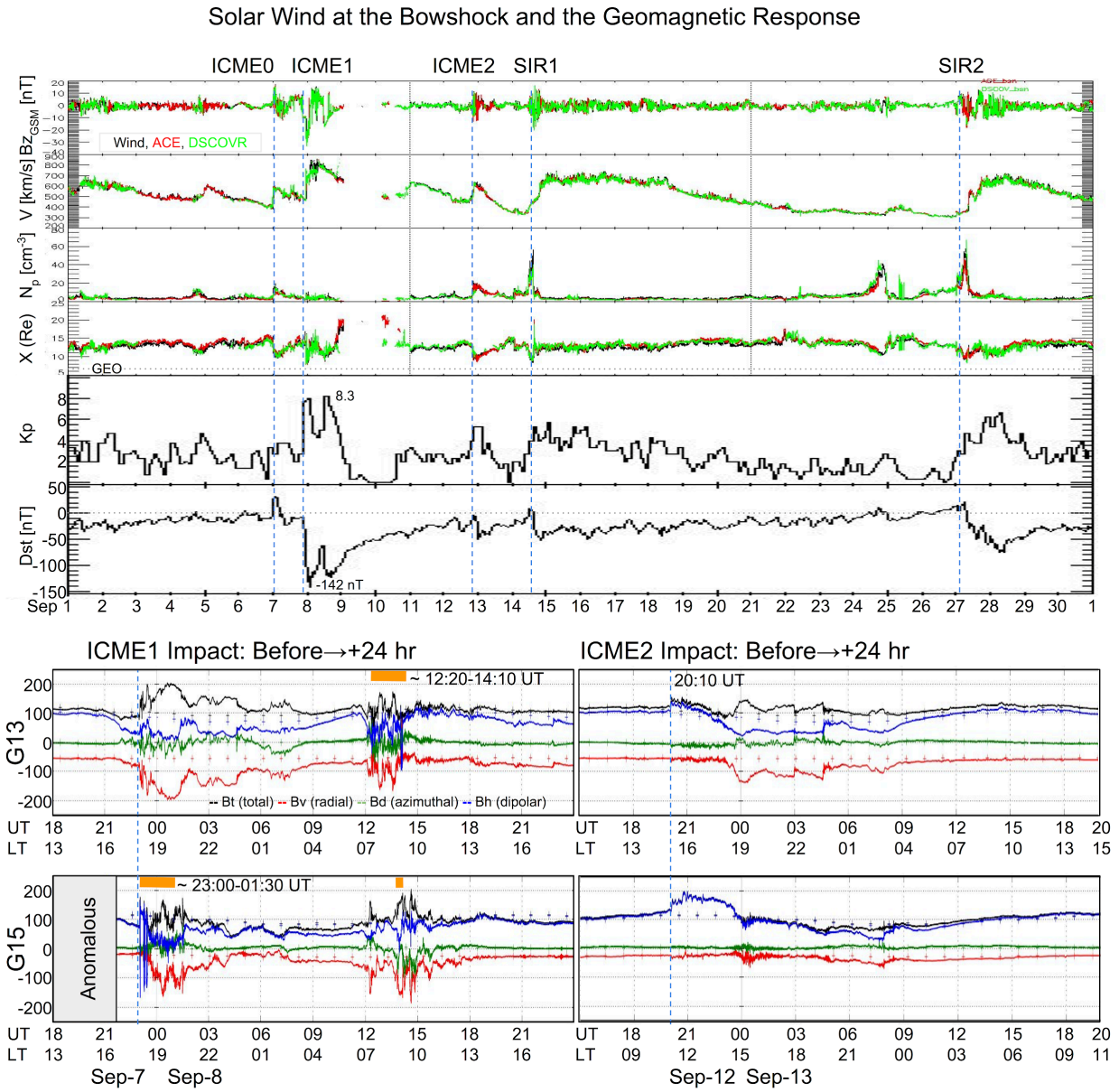

Figure 5: Solar wind at the bowshock and geomagnetic response for September, and GOES magnetic field response to ICME1 and ICME2 arrivals. The figure in the top half of this panel provides key interplanetary parameters shifted to the bowshock nose and the geomagnetic response for the full month of September (adapted from OMNIWeb) and the six plots in this panel from top to bottom are the Bz (GSM) component of the IMF, flow speed, proton density, bowshock nose distance (Re, geocentric), Kp and Dst (quick-look). The solar wind observing spacecraft (top 4 plots) are DSCOVR (green), ACE (red) and Wind (black). The approximate arrival times of key ICMEs and SIRs throughout September are labeled with dashed blue lines. At the start of the solar wind data gap Kp is ~ 2 and Dst is ~ -75 nT. The quad occupying the lower half of this panel shows the geosynchronous magnetic field response to the ICMEs arriving on 7 September (ICME1) and 12 September (ICME2) (dashed blue lines) as observed by GOES-13 and GOES-15. The coordinate frame is dipole field aligned (B_v: radial/poloidal (red), B_d: azimuthal/toroidal (green), B_h: dipolar/compressional (blue), B_t: total (black)). Plus '+'

symbols occurring hourly are the Olson-Pfitzer quiet time model (OP77; Olson and Pfitzer (1977)). Periods of dayside geosynchronous magnetopause crossings determined by $B_h < 0$ are indicated by orange bars.

4 Caribbean Radio Communication Impacts

As Caribbean communities were responding to the 2017 hurricane season, the evolving active region AR12673 erupted several times releasing X-class solar flares on September 6, 7, and 10 (Table 1). Rapid and comprehensive ionization of the equatorial upper atmosphere occurred, disrupting HF communications while emergency managers were struggling to provide critical recovery services (e.g. NCEI, 2017). Issues were reported by the Hurricane Weather Net (HWN), and the French Civil Aviation Authority (DGAC).

Several news stories from the American Radio Relay League (ARRL) convey the Caribbean radio operator perspective well. A few key excerpts are integrated here. Regarding the X9.3 flare on September 6, HWN manager Bobby Graves reports: "In addition to the mix of three hurricanes, the HWN has been hassled by a series of solar flares — one a massive Class X-9.3, said to be the most powerful flare in more than a decade. 'This solar flare caused a near-total communications blackout for most of the morning and early afternoon,' Graves recounted" (ARRL, September 6, 2017). In consideration of the X8.2 flare on September 10, he further implores: "As if Earth's weather was not bad enough already, an X-class solar flare severely disrupted HF communication on Sunday at around 1600 UTC. Graves said the widespread communication blackout lasted for nearly 3 hours, 'which could not have happened at a worse time'" (ARRL, September 11, 2017). In addition to issues experienced by ground operators, shortly after the September X9.3 solar flare, "French Civil Aviation authorities reported that HF

radio contact was lost with one non-Controller Pilot Data Link Communications (CPDLC) equipped aircraft off the coasts of Brazil and French Guyana for approximately 90 minutes, triggering an alert phase until a position report was received by New York radio" (French Civil Aviation Authority to SWPC; Rutledge and Desbios, 2018).

Figure 6 provides a graphical summary of the unfortunate alignment between terrestrial and space weather during the 2017 hurricane season. The map on the upper left shows the paths of Hurricane Irma and Jose, which were ravaging the Caribbean during the solar eruptions of AR12673. Hurricane Maria, whose eye passed directly over Puerto Rico, followed in mid to late September. The map on the bottom left shows the location of the aforementioned aircraft HF loss overlaid on the 6 September X9.3 flare radio blackout prediction using the D-Region Absorption Prediction (DRAP) product (Sauer and Wilkinson, 2008). The right column provides maps estimating the night-time lights as a power grid health proxy using the Suomi NPP Day Night Band for August (top) and for late September after hurricane Maria (bottom). Clearly, this imagery gives a bleak view of post-hurricane Puerto Rico and the rest of the Caribbean. The extraordinary sense of duty of the many relief effort contributors is well captured, once more by Graves: "Considering the poor band conditions, not to mention the solar flares, members of the Hurricane Watch Net persevered and did everything possible to help those in harm's way" (ARRL September 12, 2017).

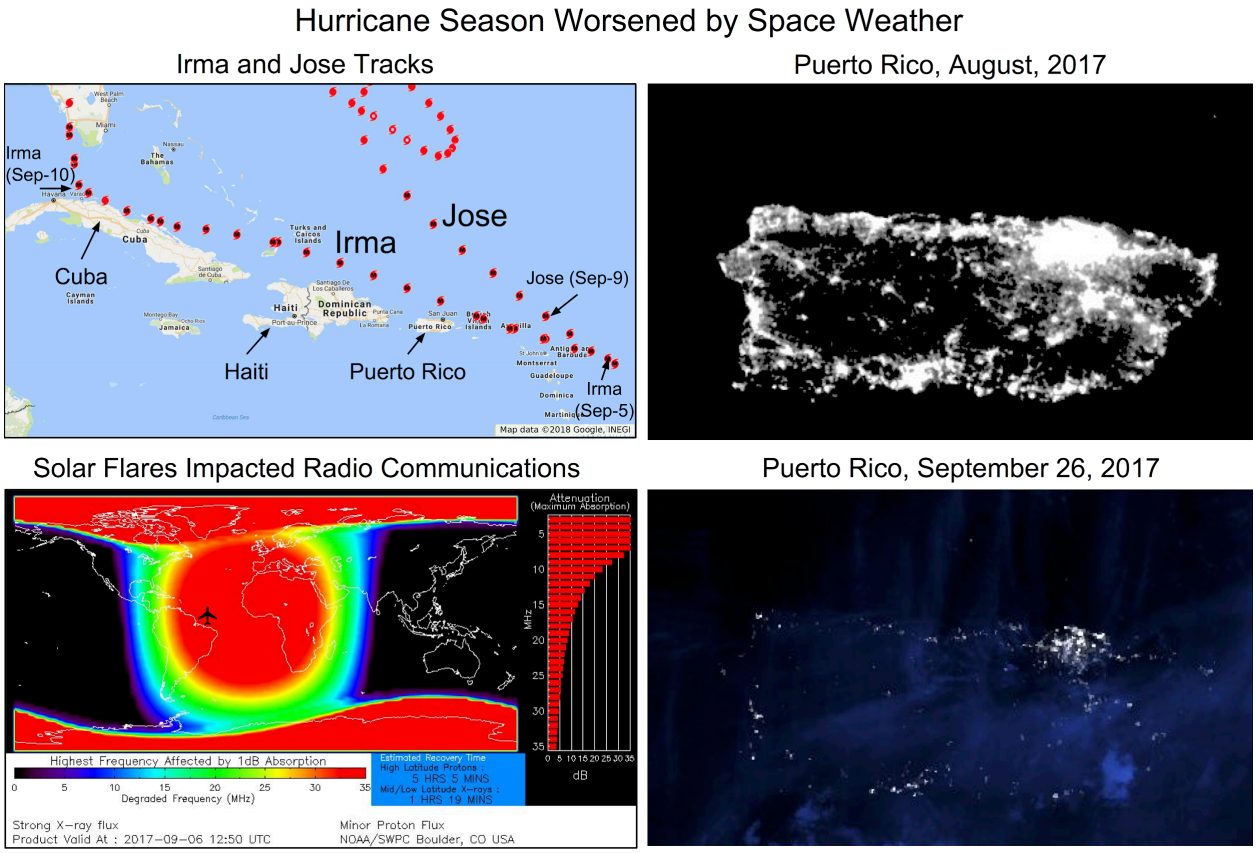

Figure 6: Hurricane season issues worsened by solar eruptions. The top left figure depicts the storm tracks of hurricanes Irma and Jose through the Caribbean (source: NWS data overlaid on Google Maps; see Table 2). The bottom left figure provides an estimate of HF radio absorption due to the 6 September solar eruption X9.3 flare and SEP using the DRAP model. The right column shows an estimate of the night-time lights as a power grid health proxy using the Suomi NPP Day Night Band for August (top) and for late September (bottom) (courtesy NCEI's Chris Elvidge and Kim Baugh).

Considering this period included the most energetic active region of solar cycle 24, with multiple X-class flares, and multiple days of SWPC forecaster alerts at "severe" and "strong" levels, it is anticipated that additional technological consequences will be reported in the future. For additional guidance evaluating the origins, predictability, and consequences of space weather events using NOAA, NASA and other research community tools, see Buzulukova (2018). In particular, evaluating potential degradations to the U.S. Wide Area Augmentation System (WAAS) and the European Geostationary Navigation Overlay Service (EGNOS) navigation aids

367 due to the geomagnetic storm (7–8 September) should be explored and is the subject of a future
368 investigation. Similar to the WAAS and EGNOS degradations concluded by Redmon et al.
369 (2018a) in their evaluation of geomagnetic storms in 2014 and 2015, maps of the Total Electron
370 Content (TEC) from the Madrigal service on September 7–8 show the development of significant
371 TEC gradients and EGNOS maps indicate service degradation relative to nearby non-storm days
372 (see Table 2 for data access).

373 ## 5 Summary

374 Multiple hurricanes carved destructive paths through the Caribbean during the 2017 hurricane
375 season, taking their toll on human life and critical infrastructure. The eyes of hurricanes Irma and
376 Jose passed slightly north of Puerto Rico, while Maria passed directly overhead. As a result, the
377 socioeconomically and technologically diverse communities of the Caribbean will collectively be
378 rebuilding and recovering for many years. This season, terrestrial and space weather collided,
379 exaggerating the consequences. AR12673 was the most energetic active region of solar cycle 24,
380 with its September 6th, X9.3 eruption, the most intense X-class flare recorded since 2005, and its
381 September 10th, X8.2 eruption, which produced the GLE 72 SEP event (most energetic since
382 2012). These solar eruptions led to geoeffective space weather impacting radio communications
383 tools used in the management of air traffic and emergency and disaster relief, complicating an
384 already extreme terrestrial weather period. We have provided an overview of the September
385 2017 space weather event, and a summary of its consequences with forecaster, post event analyst
386 and radio operator perspectives in order to aid future explorations between space weather, life
387 and technology.
388

389 Table 2: Data source locations [a]

Domain	**Platform**	**Provider**	**Access**
Solar Imagery	GOES-16	NCEI	https://www.ngdc.noaa.gov/stp/satellite/goes-r.html The SUVI data used in this study were created in a non-operational environment and are considered to be of "beta" maturity.
	SDO	NASA	http://www.jhelioviewer.org/
	SOHO	NASA	http://www.jhelioviewer.org/
Solar Wind	DSCOVR	NCEI	https://www.ngdc.noaa.gov/dscovr/portal/
	ACE, Wind, DSCOVR	NASA OMNIWeb	https://omniweb.sci.gsfc.nasa.gov/form/sc_merge_min1.html
Solar Energetic Particles	GOES SEM	NCEI	https://www.ngdc.noaa.gov/stp/satellite/goes/
	Neutron Monitors	NMDB	http://www.nmdb.eu/
Radiation Belts	GOES SEM	NCEI	https://www.ngdc.noaa.gov/stp/satellite/goes/
	POES/Metop SEM	NCEI	https://www.ngdc.noaa.gov/stp/satellite/poes/
	Belt Indices	NCEI	https://satdat.ngdc.noaa.gov/sem/poes/data/belt_indices/
Indices	Kp, Dst	NASA LASP	Dst "quick-look" and Kp (Figure 5): https://cdaweb.sci.gsfc.nasa.gov/index.html/ [This Dst "quick-look" is from WDC Kyoto]. Dst prediction: http://lasp.colorado.edu/space_weather/dsttemerin/archive/dst_2017_09.html
Ionosphere	DRAP	NCEI	https://www.ngdc.noaa.gov/stp/drap/
	Madrigal	MIT Haystack	http://madrigal.haystack.mit.edu/madrigal/experiments/2017/gps/08sep17/images/
Alerts	Radio, Radiation, Geomagnetic	SWPC	Scales: www.swpc.noaa.gov/noaa-scales-explanation Timeline: www.swpc.noaa.gov/products/notifications-timeline Alerts and Warnings Timeline: ftp.swpc.noaa.gov/pub/alerts/archive_20170901.html Events: ftp://ftp.swpc.noaa.gov/pub/indices/events/
Sun to Earth	Various	spaceweather.com	http://spaceweather.com/
Earth	DSCOVR EPIC	NASA	https://epic.gsfc.nasa.gov/?date=2017-09-12
Night Lights	Suomi NPP	NCEI	https://www.ngdc.noaa.gov/eog/interest/maria.html

Hurricane Reports	Reports	NWS	https://www.nhc.noaa.gov/data/tcr/
Aviation	WAAS	FAA	Top: http://www.nstb.tc.faa.gov/DisplayDailyPlotArchive. htm Events: http://ftp.nstb.tc.faa.gov/pub/NSTB_data/ 24HOURPLOTS/
	EGNOS	EDAS	Protection Level: https://egnos-user-support.essp-sas.eu/new_egnos_ops/ protection_level LPV200: https://egnos-user-support.essp-sas.eu/new_egnos_ops/ lpv200_availability Courtesy of ESSP and European GNSS Agency, produced under a program funded by the European Union

[a] From left to right, the columns provide: (1) domain or purpose, (2) observing platform or model, (3) provider, and (4) access method, after Redmon et al. (2018a).

Acknowledgements

Two key NOAA organizations play roles that are critical to the U.S. and international space weather programs. SWPC provides data and information about the current and future state of the space environment and hazards products during elevated space weather conditions, helping to ensure the safety of life and property. The NCEI lab in Boulder, Colorado was known for decades as the National Geophysical Data Center (NGDC) and World Data Center A (WDC-A). NCEI's Solar Terrestrial Physics program works very closely with SWPC and is currently responsible for the calibration and validation of most of NOAA's space environmental instruments, the development of new products, the archival of key operational products used by SWPC, the creation and dissemination of upgraded reference space environmental data records, and interacting with other governmental and space physics research communities to optimize the value and use of NOAA archives. The authors sincerely thank the many institutions and

individuals responsible for the Sun-to-Earth observations and predictions presented herein (see Table 2) including NASA CDAWeb's J. H. King and N. Papitashvili. The authors also wish to specifically thank these individuals for valuable discussions: Bob Rutledge (SWPC), William Rowland (NCEI DSCOVR data manager).

We acknowledge the NMDB database (www.nmdb.eu), founded under the European Union's Seventh Framework (FP7) Programme (FP/2007-2013) under contract no. 213007, for providing data. The neutron monitor data from Fort Smith are provided by the University of Delaware Department of Physics and Astronomy and the Bartol Research Institute. The data from South Pole Bares (SOPB) are provided by the University of Delaware with support from the U.S. National Science Foundation under grant ANT-0838839. Terre Adélie neutron monitor data were kindly provided by the French Polar Institute (IPEV, Brest) and by Paris Observatory. Oulu neutron monitor data were kindly provided by the Sodankyla Geophysical Observatory. The authors thank Dr Marc Duldig and the Australian Antarctic Division for providing the data from the Mawson neutron monitor.

References

ARRL, "Hurricane Watch Net Now Watching Three Atlantic Basin Hurricanes", http://www.arrl.org/news/hurricane-watch-net-now-watching-three-atlantic-basin-hurricanes, September 6, 2017.

ARRL, "Amateur Radio Volunteer Response Continues to Historic Hurricane Irma", http://www.arrl.org/news/amateur-radio-volunteer-response-continues-to-historic-hurricane-irma, September 11, 2017.

ARRL, "Hurricane Watch Net Currently Not Active but Still Eyeing José", http://www.arrl.org/news/hurricane-watch-net-currently-not-active-but-still-eyeing-jos, September 12, 2017.

Baker, D.N., Li, X., Pulkkinen, A., Ngwira, C.M., Mays, M.L., Galvin, A.B., Simunac, K.D.C., 2013. A major solar eruptive event in July 2012: defining extreme space weather scenarios. Space Weather 11 (10), 585–591. https://doi.org/10.1002/swe.20097.

Bodeau, M., 2010. High Energy Electron Climatology that Supports Deep Charging Risk Assessment in GEO, 2010–1608.

Buzulukova, N. Ed. (2018), Extreme Events in Geospace: Origins, Predictability, and Consequences, Elsevier, doi:978-0-12-812700-1.

Dichter, B. K., Galica, G. E., McGarity, J. O., Tsui, S., Golightly, M. J., Lopate, C., et al. (2015). Specification, design and calibration of the space
weather suite of instruments on the NOAA GOES-R program spacecraft. IEEE Transactions on Nuclear Science, 62(6), 2776–2783.

Farris, M.H. and C.T. Russell, Determining the standoff distance of the bow shock: Mach number dependence and use of models, J. Geophys. Res., 99, 17681-17689, 1994, doi:10.1029/94JA01020.

Huang, C.-L., H. E. Spence, and B. T. Kress (2009), Assessing access of galactic cosmic rays at Moon's orbit, *Geophys. Res. Lett.*, 36, L09109, doi:10.1029/2009GL037916.

Kuwabara, T., J. W. Bieber, J. Clem, P. Evenson, and R. Pyle (2006), Development of a ground level enhancement alarm system based upon neutron monitors, Space Weather, 4, S10001, doi:10.1029/2006SW000223.

Li, G., R. Moore, R. A. Mewaldt, L. Zhao, and A. W. Labrador (2012), A Twin-CME Scenario for Ground Level Enhancement Events, Space Sci. Rev., 171, 141–160, doi: 10.1007/s11214-011-9823-7.

Lugaz, N., M. Temmer, Y. Wang, and C. J. Farrugia (2017), The Interaction of Successive Coronal Mass Ejections: A Review, Solar Phys., 292, 64, doi:10.1007/s11207-017-1091-6.

Mishev, A., Poluianov, S., Usoskin, I., 2017. Assessment of spectral and angular characteristics of sub-GLE events using the global neutron monitor network. Journal of Space Weather and Space Climate 7, A28. https://doi.org/10.1051/swsc/2017026

NCEI, National Oceanic and Atmospheric Administration, National Centers for Environmental Information. (2017, September 17). Large Solar Event Detected During Irma. Retrieved from https://www.ncei.noaa.gov/news/large-solar-event-detected-during-irma.

Olson, W. P., and K. A. Pfitzer (1977), Magnetospheric magnetic field modeling, Annual Scientific Report, AFOSR contract F44620-75-C-0033, McDonnell Douglas Astronaut, Co.

Onsager, T. G., J. C. Green, G. D. Reeves, and H. J. Singer (2007), Solar wind and magnetospheric conditions leading to the abrupt loss of outer radiation belt electrons, *J. Geophys. Res.*, 112, A01202, doi:10.1029/2006JA011708.

Petrinec, S.M., Redmon, R.J., Rastaetter, L., 2017. Nowcasting and forecasting of the magnetopause and bow shock—a status update. Space Weather 15 (1), 36–43. https://doi.org/10.1002/2016SW001565.

Redmon, R. J., W. F. Denig, T. M. Loto'aniu, D. Fuller-Rowell 2018a, Recent Geoeffective Space Weather Events and Technological System Impacts, In: Extreme Events in Geospace, Ed. N. Buzulukova, Elsevier.

Rodriguez, J.V., Onsager, T.G., Mazur, J.E., 2010. The east-west effect in solar proton flux measurements in geostationary orbit: a new GOES capability. Geophys. Res. Lett. 37, L07109. https://doi.org/10.1029/2010GL042531.

Rutledge, R., Desbios, S. (2018), "Space weather focus: Impacts of a severe space weather event on aviation operations", World Meteorological Organization Commission for Aeronautical Meteorology (CAeM) Newsletter, Issue 1/2018, Accessed on April 13, 2018,

https://mailchi.mp/f7811e0713c9/wmo-caem-newsletter-issue-12018#Item%2019.

Seaton, D. B., and J. M. Darnel (2018), Observations of an Eruptive Solar Flare in the Extended EUV Solar Corona, The Astrophysical Journal Letters, 852(1), 0–0, doi:10.3847/2041-8213/aaa28e.

Robbrecht, E. and D. Berghmans (2004), Automated recognition of coronal mass ejections (CMEs) in near-real-time data, Astronomy and Astrophysics, 425, 1097–1106, https://doi.org/10.1051/0004-6361:20041302.

Sauer, H.H., Wilkinson, D.C., 2008. Global mapping of ionospheric HF/VHF radio wave absorption due to solar energetic protons. Space Weather 6, S12002. https://doi.org/10.1029/2008SW000399.

Schwadron et al., (2018), Update on the worsening particle radiation environment observed by CRaTER and implications for future human deep-space exploration, In Press, https://agupubs.onlinelibrary.wiley.com/doi/10.1002/2017SW001803.

"Space Weather Action Plan (SWAP)", United States Office of Science and Technology Policy, 2015. Available from: https://obamawhitehouse.archives.gov/sites/default/files/microsites/ostp/final_nationalspaceweatheractionplan_20151028.pdf, Accessed 1 January 2018.

SWPC, "Space Weather Watches, Warnings and Alerts", Available from: http://www.nws.noaa.gov/os/space/ww.shtml, Access 2 April 2018.

Suvorova, A., Dmitriev, A., Chao, J.-K., Thomsen, M., Yang, Y.-H., 2005. Necessary conditions for geosynchronous magnetopause crossings. J. Geophys. Res. 110, A01206. https://doi.org/10.1029/2003JA010079.

Temerin, M., and X. Li, A new model for the prediction of Dst on the basis of the solar wind , J. Geophys. Res., 107(A12),1472, doi:10.1029/2001JA007532, 2002.

Temerin, M., and X. Li (2006), Dst model for 1995 –2002, J. Geophys. Res., 111, A04221, doi:10.1029/2005JA011257.

Wrenn, G.L., Smith, R.J.K., 1996. Probability factors governing ESD effects in geosynchronous orbit. IEEE Trans. Nucl. Sci. 43, 2783–2789.